JACS
JOURNAL OF THE AMERICAN CHEMICAL SOCIETY
pubs.acs.org/JACS
Communication

Enhancing Entangled Two-Photon Absorption for Picosecond Quantum Spectroscopy

Ryan K. Burdick, George C. Schatz, and Theodore Goodson, III*

Cite This: https://doi.org/10.1021/jacs.1c09728
Read Online
ACCESS | Metrics & More | Article Recommendations | Supporting Information

ABSTRACT: Entangled two-photon absorption (ETPA) is known to create photoinduced transitions with extremely low light intensity, reducing the risk of phototoxicity compared to classical two-photon absorption. Previous works have predicted the ETPA cross-section, σ_e, to vary inversely with the product of entanglement time (T_e) and entanglement area (A_e), i.e., $\sigma_e \sim 1/A_eT_e$. The decreasing σ_e with increasing T_e has limited ETPA to fs-scale T_e, while ETPA applications for ps-scale spectroscopy have been unexplored. However, we show that spectral−spatial coupling, which reduces A_e as the SPDC bandwidth (σ_f) decreases, plays a significant role in determining σ_e when $T_e > \sim$100 fs. We experimentally measured σ_e for zinc tetraphenylporphyrin at several σ_f values. For type-I ETPA, σ_e increases as σ_f decreases down to 0.1 ps^{-1}. For type-II SPDC, σ_e is constant for a wide range of σ_f. With a theoretical analysis of the data, the maximum type-I σ_e would occur at σ_f = 0.1 ps^{-1} (T_e = 10 ps). At this maximum, σ_e is 1 order of magnitude larger than fs-scale σ_e and 3 orders of magnitude larger than previous predictions of ps-scale σ_e. By utilizing this spectral−spatial coupling, narrowband type-I ETPA provides a new opportunity to increase the efficiency of measuring nonlinear optical signals and to control photochemical reactions requiring ps temporal precision.

Entangled two-photon absorption (ETPA) was shown to be measurable in atoms[1,2] and organic chromophores[3] using extremely low light intensity more than a decade ago. The well-known linear absorption rate for ETPA vs photon flux significantly enhances the ETPA rate compared to the classical two-photon absorption (TPA) rate at these low light intensities.[4,5] To date, ETPA has only been performed in the fs scale of the fourth-order temporal correlation, or entanglement time, T_e. ETPA with ps T_e would be beneficial for probing chemical processes such as isomerization,[6,7] proton transfer,[8,9] water solvation,[10,11] and ligand binding/unbinding.[12,13] However, previous reports on ETPA suggest that ETPA would not be measurable practically with ps-scale T_e because the ETPA cross-section, σ_e, was predicted to decrease with increasing T_e.[14−18] Other parameters of SPDC, such as the fourth-order transverse spatial correlation, or entanglement area, A_e, may be used to counteract the effect of increasing T_e.

With spontaneous parametric down-conversion (SPDC) as the entangled photon source, the ETPA cross-section with a Gaussian frequency filter has been derived previously as[19,20]

$$\sigma_e = \frac{\sqrt{2}\,\omega_s^0\omega_i^0}{\hbar^2\varepsilon_0^2c^2A_eT_e}\frac{k_f}{(\varepsilon_f-\varepsilon_g-\omega_s^0-\omega_i^0)^2+\left(\frac{k_f}{2}\right)^2} \times \left|\sum_j \mu_{fj}\mu_{jg}T_eF[(\Delta_j - ik_j/2)T_e]\right|^2 \quad (1)$$

Here, ε_g, ε_j, and ε_f are the energies of the molecule's ground, intermediate, and final states, respectively; μ_{jg} and μ_{fj} are the transition dipole moments (TDMs) from the ground-to-intermediate and intermediate-to-final states, respectively; $\omega^0_{s/i}$ are the central frequencies of the signal/idler entangled photons, respectively; $\Delta_j = \varepsilon_j - \varepsilon_g - \omega^0_s$ is the detuning energy; and F is the plasma dispersion function. We assume a monochromatic pump. The molecule's excited states are Lorentzian broadened with line widths k_j and k_f for the intermediate and final states, respectively. Previous work showed that the lifetime of the final ETPA excited state can be calculated using the spontaneous radiative lifetime for two-photon emission.[17]

While eq 1 provides the exact σ_e dependence on T_e, a simpler probabilistic model is used to describe σ_e when the T_e dependence of the modulus squared term is negligible ($T_e >$ ~500 fs):[14]

$$\sigma_e = \frac{\delta_r}{2A_eT_e} \quad (2)$$

Here δ_r is the classical TPA cross-section. In previous theoretical[14−17] and experimental[3,21,22] reports, it was assumed that T_e can be changed while A_e remains constant. From eq 2, if A_e is constant, σ_e decreases as T_e increases. However, there exists a coupling between the spectral and spatial properties of the entangled photon wave function (see the SI).[14] To change T_e, the bandwidth of the photons from SPDC must change, which should also change A_e. While this spectral−spatial coupling has been discussed in the literature before,[23,24] how

Received: September 13, 2021

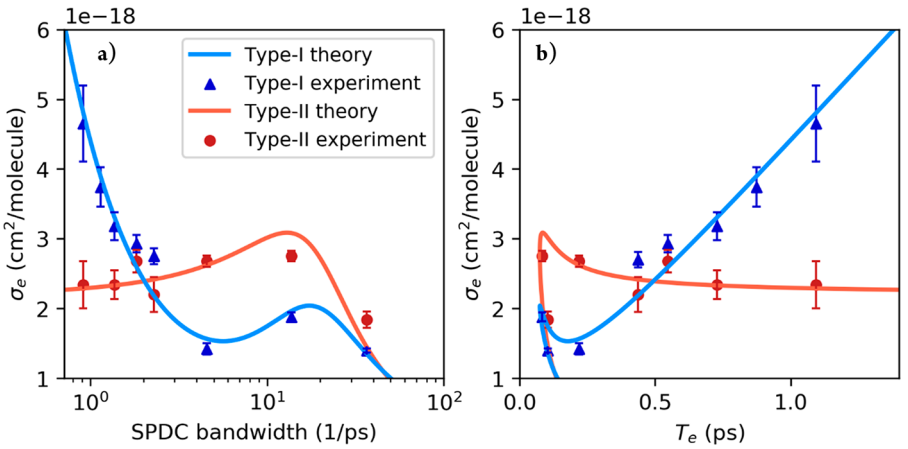

Figure 1. (a) Experimental and theoretical type-I and type-II ETPA cross-sections, σ_e, vs σ_f for a ∼20 μM solution of zinc tetraphenylporphyrin (ZnTPP). (b) Same as (a) with the *x*-axis converted to T_e.

the coupling affects the ETPA cross-section has not been considered nor explored experimentally.

Here we consider the effect of a spectral filter, with bandwidth σ_f, that is applied to the SPDC photons after they emerge from the SPDC process. Full details of our experimental setup have been reported previously[25] and can be found in the SI. In Figure 1a, the experimental σ_e for type-I and type-II filtered SPDC are plotted as a function of σ_f ranging from 0.9 to 40 ps^{-1}. In our passive filtering technique, where SPDC photons are produced in a crystal and filtered after their generation, the input photon rate for ETPA decreases with decreasing σ_f. We found that we can choose σ_f as small as 0.9 ps^{-1} before the input rate was too small to measure an ETPA signal. Due to the limited wavelength detection range of APDs, we could not obtain σ_e at σ_f > 40 ps^{-1}. Given that eqs 1 and 2 show that σ_e varies inversely with T_e, it is of interest to convert Figure 1a to show dependence on T_e (Figure 1b). Standard filter theories show that T_e varies inversely with σ_f,[26−28] which can be controlled by the bandwidth of a filter or monochromator. Dispersion was considered when calculating T_e (see SI). The smooth curves in this figure are the results of an analytical theory that we describe below.

The experimental data in Figure 1 show that for type-I SPDC at small σ_f, σ_e increases as σ_f decreases (T_e increases). For type-II SPDC at small σ_f, σ_e is constant as σ_f decreases. Not only do the two SPDC types differ from each other in their cross-section trends, they are also incompatible with the constant A_e prediction that σ_e should decrease as σ_f decreases. We note that dispersion leads to two branches in the curves in Figure 1b: an upper branch corresponding to small σ_f in which T_e is determined by $T_e = 1/\sigma_f$ and a lower branch corresponding to large σ_f where dispersion dominates, and T_e is proportional to σ_f. Figure 1 shows that both branches are involved in the data fit. However, we are only concerned with the small σ_f branch. Even with dispersion considered, the variation of σ_e with σ_f is not explained by the assumption of a constant A_e. We then consider the spectral−spatial coupling and how changing σ_f would change A_e. The solid curves in Figure 1 are the theoretical model in eq 1 including the spectral−spatial coupling explained below.

The origin of A_e is the uncertainty in the SPDC emission angles from the crystal source, as determined by the polar and azimuthal entanglement angles, θ^e and φ^e, respectively.[29,30] Because each frequency within the SPDC frequency superposition experiences a different refractive index inside the crystal, each frequency propagates at a different angle. Therefore, uncertainty in the frequency causes an uncertainty in the propagation angle and ultimately the spatial position. Decreasing the frequency uncertainty (σ_f) is then expected to decrease A_e, which should increase σ_e. However, decreasing σ_f also increases T_e, which should decrease σ_e. From the experimental data in Figure 1a, for type-II SPDC, these competing effects cancel each other, leaving σ_e constant for small σ_f. For type-I SPDC, the decreasing A_e outweighs the increasing T_e, resulting in a net increase in σ_e. We propose the following relationships between A_e and the SPDC frequency bandwidth (for small σ_f) for type-I (eq 3) and type-II (eq 4) (see SI for more details):

$$A_e = \left(\frac{\alpha}{\sigma_f^2} + \frac{\beta}{\sigma_L^2}\right)^{-1} + A_d \propto (\alpha T_{e,f}^2 + \beta T_{e,L}^2)^{-1} + A_d \tag{3}$$

$$A_e = \left(\frac{\gamma}{\sigma_f} + \frac{\zeta}{\sigma_L}\right)^{-1} + A_d \propto (\gamma T_{e,f} + \zeta T_{e,L})^{-1} + A_d \tag{4}$$

σ_L is the SPDC bandwidth emitted by the crystal with length, L, and represents the upper limit for σ_f in our experiment. $T_{e,L}$ is the corresponding entanglement time. The term A_d recognizes that there is a lower bound to A_e that is determined by diffraction. The coefficients α, β, γ, and ζ are solved for by fitting with the experimental data in Figure 1. Substituting eqs 3 and 4 into eq 2 provides new probabilistic models (to highest order in T_e) for type-I (eq 5) and type-II (eq 6) ETPA, respectively:

$$\sigma_e \propto \delta_r T_{e,f} \tag{5}$$

$$\sigma_e \propto \delta_r \tag{6}$$

Equations 5 and 6 predict the σ_e vs T_e trends (for small σ_f) that we see with the experimental data in Figure 1b for both SPDC types. To confirm the validity of eqs 5 and 6, we substitute the equations into eq 1 and fit the resulting equations with our experimental data to determine the coefficient values and extract A_e. See the SI for calculation parameters. The models are accurate until σ_f decreases to the

https://doi.org/10.1021/jacs.1c09728
J. Am. Chem. Soc. XXXX, XXX, XXX−XXX

point where A_e reaches A_d, as determined by eqs 3 and 4, which we calculate below to occur around T_e = 10 ps.

The resulting fits in Figure 1 agree reasonably well with the experimental data. The trends for $\sigma_f < 5$ ps^{-1} are the same if a sinc SPDC spectrum is considered (see the SI). For $\sigma_f > 10$ ps^{-1}, dispersion significantly increases T_e and decreases σ_e (bottom branch in Figure 1b). For σ_f in the range 0.9−40 ps^{-1}, the type-I A_e ranges from 1.95×10^{-7} to 7.39×10^{-6} cm^2, and the type-II A_e ranges from 4.12×10^{-7} to 6.91×10^{-6} cm^2. These ranges are within an order of magnitude of the assumption of $A_e = 1 \times 10^{-6}$ cm^2 in previous theoretical works for fs-scale T_e.[14,16,17]

Figure 2 shows how the type-I ETPA cross-section changes as the SPDC bandwidth is decreased until A_e reaches the diffraction limit ($(\lambda/2)^2 = 1.6 \times 10^{-9}$cm^2). For comparison, the same theoretical model (eq 1) but using a constant A_e is shown.

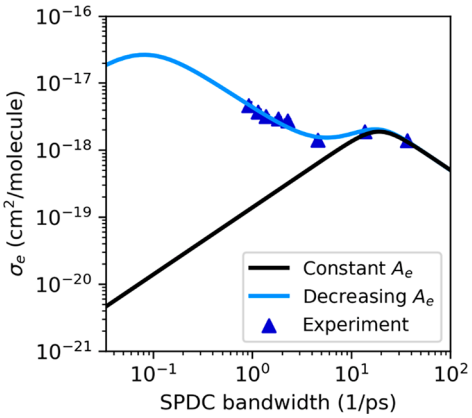

Figure 2. Comparison of the type-I ETPA experimental data with the theoretical model (eq 1) for constant A_e (black) and decreasing A_e (blue).

In Figure 2, at the smallest experimental bandwidth (0.9 ps^{-1}), the model with a constant A_e is more than an order of magnitude smaller than the experimental value. For the decreasing A_e, the maximum occurs at σ_f = 0.1 ps^{-1} (T_e = 10 ps), and here σ_e is $\sim 3 \times 10^{-17}$ cm^2, which is over 3 orders of magnitude larger than what the constant A_e predicts. Comparison of ETPA with one-photon absorption (OPA) at the intermediate state has previously been explored.[20,31,32] In this report, we considered a molecular system where the intermediate states are far off-resonance with the single photon energies, such that OPA at the intermediate states is negligible. At the maximum, σ_e for ZnTPP is within an order of magnitude of its final-state OPA cross-section ($\sim 2 \times 10^{-16}$ cm^2/molecule at 405 nm),[33] rather than 2 orders of magnitude smaller in the tens of ps^{-1} range where ETPA experiments are performed today.[43−45] To obtain enough narrowband photons to measure an ETPA signal at $\sigma_f < 0.9$ ps^{-1}, an active filtering technique using a cavity-enhanced SPDC source would be useful.[34] The SPDC photons can have a σ_f of MHz or smaller,[35−40] making T_e as large as 1 μs for visible wavelengths.[41] Alternatively, passive filtering of a periodically poled SPDC source could be used since they can provide a 3 orders of magnitude larger SPDC rate while using the same pump power as our thin crystal source.[42]

In the SI, experimental ETPA cross-sections for flavin dinucleotide (FAD) are provided, showing the same cross-section trends as ZnTPP for type-I and type-II SPDC. For these chromophores, which are much smaller than A_e in the experiment and the diffraction-limited A_e, the T_e with the maximum ETPA cross-section in the ps regime is determined by the diffraction limit of the SPDC, not the molecule. This means that any molecule of this size can receive this enhancement to its ETPA cross-section, which is useful for label-free sensing and imaging by decreasing A_e to enhance the signal from the target molecule. For analytes that are much larger in size, such as a large protein or organelle within a cell, the T_e with maximum ETPA cross-section may depend on the analyte itself. In that case, ETPA could be a new means of measuring the size of a molecule in a cell. This relationship between the size of the absorbing molecule and its ETPA cross-section will be explored in future work.

A_e at the maximum σ_e is more than 3 orders of magnitude smaller than A_e at the fs-scale T_e (see SI). This much smaller A_e would improve the spatial resolution of ETPA microscopy by more than 3 orders of magnitude, while also yielding brighter images due to the enhanced σ_e.[22] This enhancement would also provide chemists the ability to measure nonlinear optical signals, which are notoriously much weaker than linear signals, with the same absorption efficiency as linear OPA. Chemists could then more easily identify, for example, molecules with efficient charge transfer for solar cells or OLEDs.

Most interestingly, ETPA at ps-scale T_e provides a new opportunity to control chemical reactions that require intermediate conversion processes with fs−ps times, such as an isomerization, proton transfer, or intersystem crossing to a triplet state. A primary example is the photochemical reactivity of T_n triplet states in green fluorescence proteins (GFPs).[43,44] With ps T_e ETPA, the first photon would excite the GFP to the S_1 state and allow the population to cross to the T_1 state, and then the second photon would excite the GFP to the T_n state. Entangled photons are unique in that they can provide high-frequency resolution simultaneously with the required temporal resolution.[45] Classical ps laser pulses are Fourier limited, so they would lack frequency resolution in this photochemical reaction. Since excited states become closer in energy as the energy increases, maintaining high-frequency resolution with temporal resolution is crucial for control over the photochemical reaction.

■ ASSOCIATED CONTENT

Supporting Information

The Supporting Information is available free of charge at https://pubs.acs.org/doi/10.1021/jacs.1c09728.

Calculation of entanglement time with dispersion effects; origin and derivation of entanglement area as a function of entanglement time; experimental details; ETPA cross-section measurements in flavin adenine dinucleotide; effect of vibrational relaxation and of molecular motion (PDF)

■ AUTHOR INFORMATION

Corresponding Author

Theodore Goodson, III − *Department of Chemistry, University of Michigan, Ann Arbor, Michigan 48109-1055, United States;* orcid.org/0000-0003-2453-2290; Email: tgoodson@umich.edu

https://doi.org/10.1021/jacs.1c09728
J. Am. Chem. Soc. XXXX, XXX, XXX−XXX

Authors

Ryan K. Burdick − *Department of Chemistry, University of Michigan, Ann Arbor, Michigan 48109-1055, United States;* Present Address: 711th Human Performance Wing, Air Force Research Laboratory, Wright-Patterson AFB, Ohio 45433, United States; orcid.org/0000-0002-3249-7993

George C. Schatz − *Department of Chemistry, Northwestern University, Evanston, Illinois 60208-3113, United States;* orcid.org/0000-0001-5837-4740

Complete contact information is available at: https://pubs.acs.org/10.1021/jacs.1c09728

Notes

The authors declare no competing financial interest.

■ ACKNOWLEDGMENTS

This work was based on work supported by the National Science Foundation through Grant CHE-1836374 (TGIII) and by the Air Force Office of Scientific Research (Biophysics) Grant No. FA9550-20-1-0380 (TGIII). G.C.S. was supported by NSF Grant CHE-2055565. We thank Oleg Varnavski, Gyeongwon Kevin Kang, and Kobra A. Nasiri for helpful conversations.

■ REFERENCES

(1) Dayan, B.; Pe'er, A.; Friesem, A. A.; Silberberg, Y. Two Photon Absorption and Coherent Control with Broadband Down-Converted Light. *Phys. Rev. Lett.* **2004**, *93* (2), 023005.

(2) Dayan, B.; Pe'er, A.; Friesem, A. A.; Silberberg, Y. Nonlinear Interactions with an Ultrahigh Flux of Broadband Entangled Photons. *Phys. Rev. Lett.* **2005**, *94* (4), 043602.

(3) Lee, D.-I.; Goodson, T. Entangled Photon Absorption in an Organic Porphyrin Dendrimer. *J. Phys. Chem. B* **2006**, *110* (51), 25582−25585.

(4) Javanainen, J.; Gould, P. L. Linear intensity dependence of a two-photon transition rate. *Phys. Rev. A: At., Mol., Opt. Phys.* **1990**, *41* (9), 5088−5091.

(5) Harpham, M. R.; Süzer, Ö.; Ma, C.-Q.; Bäuerle, P.; Goodson, T. Thiophene Dendrimers as Entangled Photon Sensor Materials. *J. Am. Chem. Soc.* **2009**, *131* (3), 973−979.

(6) Jung, Y. O.; Lee, J. H.; Kim, J.; Schmidt, M.; Moffat, K.; Šrajer, V.; Ihee, H. Volume-conserving trans−cis isomerization pathways in photoactive yellow protein visualized by picosecond X-ray crystallography. *Nat. Chem.* **2013**, *5* (3), 212−220.

(7) Zheng, J.; Kwak, K.; Xie, J.; Fayer, M. D. Ultrafast Carbon-Carbon Single-Bond Rotational Isomerization in Room-Temperature Solution. *Science* **2006**, *313* (5795), 1951.

(8) Zhang, Y.; de La Harpe, K.; Beckstead, A. A.; Improta, R.; Kohler, B. UV-Induced Proton Transfer between DNA Strands. *J. Am. Chem. Soc.* **2015**, *137* (22), 7059−7062.

(9) Stoner-Ma, D.; Jaye, A. A.; Matousek, P.; Towrie, M.; Meech, S. R.; Tonge, P. J. Observation of Excited-State Proton Transfer in Green Fluorescent Protein using Ultrafast Vibrational Spectroscopy. *J. Am. Chem. Soc.* **2005**, *127* (9), 2864−2865.

(10) Li, T.; Hassanali, A. A.; Kao, Y.-T.; Zhong, D.; Singer, S. J. Hydration Dynamics and Time Scales of Coupled Water−Protein Fluctuations. *J. Am. Chem. Soc.* **2007**, *129* (11), 3376−3382.

(11) Pham, V.-T.; Penfold, T. J.; van der Veen, R. M.; Lima, F.; El Nahhas, A.; Johnson, S. L.; Beaud, P.; Abela, R.; Bressler, C.; Tavernelli, I.; Milne, C. J.; Chergui, M. Probing the Transition from Hydrophilic to Hydrophobic Solvation with Atomic Scale Resolution. *J. Am. Chem. Soc.* **2011**, *133* (32), 12740−12748.

(12) Kim, S.; Lim, M. Picosecond Dynamics of Ligand Interconversion in the Primary Docking Site of Heme Proteins. *J. Am. Chem. Soc.* **2005**, *127* (16), 5786−5787.

(13) Kim, S.; Lim, M. Protein Conformation-Induced Modulation of Ligand Binding Kinetics: A Femtosecond Mid-IR Study of Nitric Oxide Binding Trajectories in Myoglobin. *J. Am. Chem. Soc.* **2005**, *127* (25), 8908−8909.

(14) Fei, H.-B.; Jost, B. M.; Popescu, S.; Saleh, B. E. A.; Teich, M. C. Entanglement-Induced Two-Photon Transparency. *Phys. Rev. Lett.* **1997**, *78* (9), 1679−1682.

(15) Saleh, B. E. A.; Jost, B. M.; Fei, H.-B.; Teich, M. C. Entangled-Photon Virtual-State Spectroscopy. *Phys. Rev. Lett.* **1998**, *80* (16), 3483−3486.

(16) Burdick, R. K.; Varnavski, O.; Molina, A.; Upton, L.; Zimmerman, P.; Goodson, T. Predicting and Controlling Entangled Two-Photon Absorption in Diatomic Molecules. *J. Phys. Chem. A* **2018**, *122* (41), 8198−8212.

(17) Kang, G.; Nasiri Avanaki, K.; Mosquera, M. A.; Burdick, R. K.; Villabona-Monsalve, J. P.; Goodson, T.; Schatz, G. C. Efficient Modeling of Organic Chromophores for Entangled Two-Photon Absorption. *J. Am. Chem. Soc.* **2020**, *142* (23), 10446−10458.

(18) Mukamel, S.; Freyberger, M.; Schleich, W.; Bellini, M.; Zavatta, A.; Leuchs, G.; Silberhorn, C.; Boyd, R. W.; Sánchez-Soto, L. L.; Stefanov, A.; Barbieri, M.; Paterova, A.; Krivitsky, L.; Shwartz, S.; Tamasaku, K.; Dorfman, K.; Schlawin, F.; Sandoghdar, V.; Raymer, M.; Marcus, A.; Varnavski, O.; Goodson, T.; Zhou, Z.-Y.; Shi, B.-S.; Asban, S.; Scully, M.; Agarwal, G.; Peng, T.; Sokolov, A. V.; Zhang, Z.-D.; Zubairy, M. S.; Vartanyants, I. A.; del Valle, E.; Laussy, F. Roadmap on quantum light spectroscopy. *J. Phys. B: At., Mol. Opt. Phys.* **2020**, *53* (7), 072002.

(19) de J León-Montiel, R.; Svozilík, J.; Salazar-Serrano, L. J.; Torres, J. P. Role of the spectral shape of quantum correlations in two-photon virtual-state spectroscopy. *New J. Phys.* **2013**, *15* (5), 053023.

(20) Nakanishi, T.; Kobayashi, H.; Sugiyama, K.; Kitano, M. Full Quantum Analysis of Two-Photon Absorption Using Two-Photon Wave Function: Comparison of Two-Photon Absorption with One-Photon Absorption. *J. Phys. Soc. Jpn.* **2009**, *78* (10), 104401.

(21) Varnavski, O.; Pinsky, B.; Goodson, T. Entangled Photon Excited Fluorescence in Organic Materials: An Ultrafast Coincidence Detector. *J. Phys. Chem. Lett.* **2017**, *8* (2), 388−393.

(22) Varnavski, O.; Goodson, T. Two-Photon Fluorescence Microscopy at Extremely Low Excitation Intensity: The Power of Quantum Correlations. *J. Am. Chem. Soc.* **2020**, *142* (30), 12966−12975.

(23) Zeilinger, A. Experiment and the foundations of quantum physics. *Rev. Mod. Phys.* **1999**, *71* (2), S288−S297.

(24) Yin, L.; Li, J.; Zhai, W.; Xia, M.; Hu, Y.; Zheng, X. Analysis of the Spatial Properties of Correlated Photon in Collinear Phase-Matching. *Photonics* **2021**, *8* (1), 12.

(25) Villabona-Monsalve, J. P.; Burdick, R. K.; Goodson, T. Measurements of Entangled Two-Photon Absorption in Organic Molecules with CW-Pumped Type-I Spontaneous Parametric Down-Conversion. *J. Phys. Chem. C* **2020**, *124* (44), 24526−24532.

(26) Kim, Y.-H. Measurement of one-photon and two-photon wave packets in spontaneous parametric downconversion. *J. Opt. Soc. Am. B* **2003**, *20* (9), 1959−1966.

(27) Campos, R. A.; Saleh, B. E. A.; Teich, M. C. Fourth-order interference of joint single-photon wave packets in lossless optical systems. *Phys. Rev. A: At., Mol., Opt. Phys.* **1990**, *42* (7), 4127−4137.

(28) Rubin, M. H.; Klyshko, D. N.; Shih, Y. H.; Sergienko, A. V. Theory of two-photon entanglement in type-II optical parametric down-conversion. *Phys. Rev. A: At., Mol., Opt. Phys.* **1994**, *50* (6), 5122−5133.

(29) Joobeur, A.; Saleh, B. E. A.; Larchuk, T. S.; Teich, M. C. Coherence properties of entangled light beams generated by parametric down-conversion: Theory and experiment. *Phys. Rev. A: At., Mol., Opt. Phys.* **1996**, *53* (6), 4360−4371.

(30) Joobeur, A.; Saleh, B. E. A.; Teich, M. C. Spatiotemporal coherence properties of entangled light beams generated by parametric down-conversion. *Phys. Rev. A: At., Mol., Opt. Phys.* **1994**, *50* (4), 3349−3361.

(31) Oka, H. Two-photon absorption by spectrally shaped entangled photons. *Phys. Rev. A: At., Mol., Opt. Phys.* **2018**, *97* (3), 033814.
(32) Oka, H. Enhanced vibrational-mode-selective two-step excitation using ultrabroadband frequency-entangled photons. *Phys. Rev. A: At., Mol., Opt. Phys.* **2018**, *97* (6), 063859.
(33) Dixon, J. M.; Taniguchi, M.; Lindsey, J. S. PhotochemCAD 2: A Refined Program with Accompanying Spectral Databases for Photochemical Calculations¶. *Photochem. Photobiol.* **2005**, *81* (1), 212−213.
(34) Slattery, O.; Ma, L.; Zong, K.; Tang, X. Background and Review of Cavity-Enhanced Spontaneous Parametric Down-Conversion. *Journal of Research of the National Institute of Standards and Technology* **2019**, *124*, 1−18.
(35) Tomoyuki, H. Quantum key distribution with mode-locked two-photon states. *2015 Conference on Lasers and Electro-Optics Pacific Rim* 2015; 27P_41.
(36) Fekete, J.; Rieländer, D.; Cristiani, M.; de Riedmatten, H. Ultranarrow-Band Photon-Pair Source Compatible with Solid State Quantum Memories and Telecommunication Networks. *Phys. Rev. Lett.* **2013**, *110* (22), 220502.
(37) Kuklewicz, C. E.; Wong, F. N. C.; Shapiro, J. H. Time-Bin-Modulated Biphotons from Cavity-Enhanced Down-Conversion. *Phys. Rev. Lett.* **2006**, *97* (22), 223601.
(38) Ou, Z. Y.; Lu, Y. J. Cavity Enhanced Spontaneous Parametric Down-Conversion for the Prolongation of Correlation Time between Conjugate Photons. *Phys. Rev. Lett.* **1999**, *83* (13), 2556−2559.
(39) Polzik, J. S. N.-N. a. B. M. N. a. H. T. a. A. I. V. a. E. S. High purity bright single photon source. *Opt. Express* **2007**, *15* (13), 7940−7949.
(40) Bao, X.-H.; Qian, Y.; Yang, J.; Zhang, H.; Chen, Z.-B.; Yang, T.; Pan, J.-W. Generation of Narrow-Band Polarization-Entangled Photon Pairs for Atomic Quantum Memories. *Phys. Rev. Lett.* **2008**, *101* (19), 190501.
(41) Liu, J.; Liu, J.; Yu, P.; Zhang, G. Sub-megahertz narrow-band photon pairs at 606 nm for solid-state quantum memories. *APL Photonics* **2020**, *5* (6), 066105.
(42) Jabir, M. V.; Samanta, G. K. Robust, high brightness, degenerate entangled photon source at room temperature. *Sci. Rep.* **2017**, *7* (1), 12613.
(43) Byrdin, M.; Duan, C.; Bourgeois, D.; Brettel, K. A Long-Lived Triplet State Is the Entrance Gateway to Oxidative Photochemistry in Green Fluorescent Proteins. *J. Am. Chem. Soc.* **2018**, *140* (8), 2897−2905.
(44) Mohr, M. A.; Kobitski, A. Y.; Sabater, L. R.; Nienhaus, K.; Obara, C. J.; Lippincott-Schwartz, J.; Nienhaus, G. U.; Pantazis, P. Rational Engineering of Photoconvertible Fluorescent Proteins for Dual-Color Fluorescence Nanoscopy Enabled by a Triplet-State Mechanism of Primed Conversion. *Angew. Chem., Int. Ed.* **2017**, *56* (38), 11628−11633.
(45) Schlawin, F.; Dorfman, K. E.; Mukamel, S. Entangled Two-Photon Absorption Spectroscopy. *Acc. Chem. Res.* **2018**, *51* (9), 2207−2214.

https://doi.org/10.1021/jacs.1c09728
J. Am. Chem. Soc. XXXX, XXX, XXX−XXX